Thermal Performance of Alternating-Current Heat Recovery Ventilator in Partially Wet Conditions

Ahmad Alfan Farizi
Graduate School of Mechanical Engineering, College of Engineering, Kookmin University

Hyunjin Lee
Department of Mechanical Engineering, College of Engineering, Kookmin University

Hwataik Han
Department of Mechanical Engineering, College of Engineering, Kookmin University

https://doi.org/10.5109/4372282

出版情報：Evergreen. 8 (1), pp.221-228, 2021-03. Transdisciplinary Research and Education Center for Green Technologies, Kyushu University
バージョン：

Thermal Performance of Alternating-Current Heat Recovery Ventilator in Partially Wet Conditions

Ahmad Alfan Farizi[1], Hyunjin Lee[2], Hwataik Han[2,*]

[1]Graduate School of Mechanical Engineering, College of Engineering, Kookmin University, Seoul 02707, Republic of Korea

[2]Department of Mechanical Engineering, College of Engineering, Kookmin University, Seoul 02707, Republic of Korea

*Author to whom correspondence should be addressed:
E-mail: hhan@kookmin.ac.kr

(Received October 30, 2020; Revised March 26, 2021; accepted March 26, 2021).

Abstract: This paper investigates the effect of moisture transfer on the thermal performance of an alternating-current heat recovery ventilator (AC-HRV). Contrary to conventional direct-current ventilation in two separate ducts, alternating-current ventilation periodically changes its airflow directions in a single duct. Exhaust energy is stored and recovered in and out of the thermal storage unit during charging and discharging processes. A theoretical model has been developed to obtain the transient temperature and humidity distributions inside a thermal storage unit in partially wet conditions. Based on the distributions, the thermal performance of the HRV is analyzed at cyclic steady states. Results show complicated patterns of moisture condensation and evaporation during an entire period of charging and discharging processes. The maximum thickness of water condensate is 2.67 μm, which is negligible under the present test conditions. The enthalpy efficiency of an AC-HRV increases as the accumulated mass of condensate increases due to the latent heat.

Keywords: evergreen; Heat recovery ventilator, Alternating-current ventilation, Enthalpy efficiency, Condensation

1. Introduction and Background

As people spend most of their time indoors in houses and workplaces[1)], indoor air quality becomes a crucial factor for their performance and productivity as well as their comfort and health[2)]. It is essential to provide an adequate amount of fresh air [3)] to create a comfortable and healthy indoor environment[4, 5)]. Heat recovery ventilators (HRVs) are frequently used[6)] in order to save ventilation energy. Proper design of HRV systems can provide quality indoor air and save heating and cooling loads[7)]. There are several types of commonly used HRVs (e.g., flat plate, rotary wheel, heat pipe, and run-around types[8, 9)]). Conventional ventilators require two sets of inlet and outlet air ducts to exchange energy simultaneously[10)]. These air ducts and HRV systems are usually located above the ceiling panel. Ductworks can be complicated and troublesome when the building does not have enough space above the ceiling panel[11)].

A new concept of HRV system has been proposed, namely alternating-current HRV (AC-HRV), which works similar to human respiration[12)]. During exhalation, the warm air heats the respiratory tract as it passes through it whereas, during inhalation, cold outside air is warmed up by the respiratory tract that has been heated during exhalation. The same principle is used in an AC-HRV, which has the advantage of using a single-duct system for both supply and exhaust purposes[13)]. Thermal storage material is charged during the exhaust process and is discharged during the supply process. In a sense, this is similar to a rotary-type HRV. Instead of swapping the matrix position by rotating a wheel, the airflow direction is reversed with the matrix fixed at a certain position.

Extensive studies have been conducted to investigate the effect of the system parameters on HRV performance[14)], the optimization strategy for ventilation[15)], and the effect of phase changes in heat exchangers[16)]. A series of papers that analytically evaluated the efficiency of heat recovery, with the inclusion of the effects of condensation[17)] and frost formation[18)], were published. Experiments were conducted for a parametric study on sensible plate heat exchangers under condensation conditions[19, 20)]. As the inlet humidity level is increased, the heat transfer rate was observed to increase with an increase in the amount of condensed water[21, 22)]. A simplified numerical model for internal condensation, which can be used along with CFD calculations, has been proposed and applied to a flat-plate-type heat recovery

ventilator in partially wet conditions[23].

There are only a few studies to investigate the heat transfer characteristics of a thermal storage medium for an AC-HRV system. Experiments have been done to validate the cyclic heat transfer model for AC-HRVs only for dry conditions[24, 25].

This paper numerically investigates the effect of water vapor condensation and evaporation on an AC-HRV thermal storage unit composed of mini square channels on the efficiency of the HRV.

2. Method

2.1 Thermal storage model

The thermal storage model used in this study is a collection of multiple square channels, as shown in Fig. 1. The channel walls are made of thermal storage material. A charging process takes place during the first half-period (t_p), and a discharging process follows with the flow direction reversed for the next half-period; this continues periodically and alternately. Table 1 shows the specifications of the thermal storage unit. The thermal storage material used in this study is made of aluminum oxide and silicon oxide(Al2O3 61%, SiO2 29.3%, MgO 3.82%, TiO2 2.34%, Fe2O3 1.08%, CaO 1.08%), whose properties are shown in Table 2.

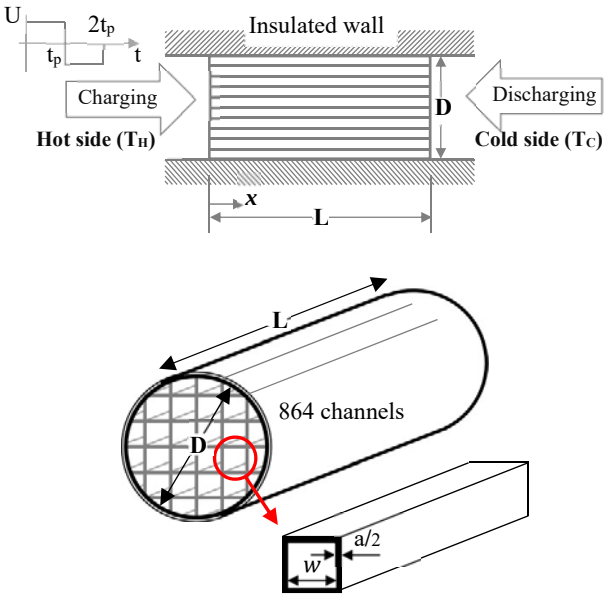

Fig. 1: Thermal storage unit for AC-HRV

Table 1. Specifications of thermal storage unit

Properties	Value
Diameter, D	0.15 m
Length, L	1 m
Air passage, w	3.4 mm
Wall thickness, a	1 mm
Solid mass per unit length, Ms/L	13.8 kg/m

Table 2. Properties of thermal storage material

Properties	Value
Density, ρ_s	1958 kg/m^3
Heat capacity, C_{ps}	757 J/kg/°C
Thermal conductivity, k_s	36 W/m/°C

Table 3. Reference conditions

Variables	Value
Air velocity, U	5.24 m/s
Mass flow rate of dry air, $\dot{m}_a$	0.065 kg/s
Half-period, t_p	120 s

Table 4. Indoor and outdoor temperature and humidity

Variables	Value
Indoor temperature, T_H	22 °C
Outdoor temperature, T_C	0 °C
Indoor relative humidity, RH_{in}	50%
Outdoor relative humidity, RH_{out}	50%

The reference operating conditions for this study are shown in Table 3. The air velocity corresponds to 200 CMH of HRV airflow rate. The half-period is 2 minutes. The indoor and outdoor conditions are shown in Table 4.

2.2 Governing equations

Assumptions have been made to derive governing equations as follows.

- Constant thermal properties of air and solid material
- Uniform air velocity in a channel
- Constant heat/mass transfer coefficients on surfaces
- Negligible volume of condensed liquid water

The mass balance and energy balance equations can be written as Eq. 1 and Eq. 2[12, 26]. The heat and moisture transfer rates are positive for the cooling and condensation processes, and negative for the heating and evaporation processes.

$$\dot{m}_a W_2 = \dot{m}_a W_1 - \dot{m}_w \qquad (1)$$

$$\dot{m}_a i_2 = \dot{m}_a i_1 - \dot{q} - \dot{m}_w i_{fg} \qquad (2)$$

When hot and humid air passes over the surface of the thermal storage during a charging period, condensation occurs on the surface when the solid temperature is below its dew-point temperature. During a discharging period, when cold and dry outdoor air passes over the warm and wet surface of thermal storage, the air is warmed and humidified by the evaporation from the surface. If the surface is dried out, only sensible heat transfer takes place. Fig. 2 shows schematics of heat and moisture transfer during the charging and discharging processes.

The boundary conditions for periodically repeated charging and discharging processes are:

- Charging process $(0 < t < t_p)$;
  $u(t,0) = U \qquad T_f(t,0) = T_H \qquad W(t,0) = W_H$
- Discharging process $(t_p < t < 2t_p)$;

$$u(t,L) = -U \qquad T_f(t,L) = T_C \qquad W(t,L) = W_C$$

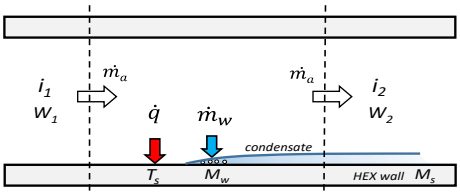

(a) Charging process

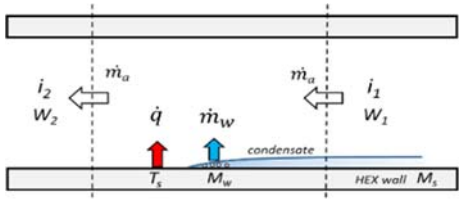

(b) Discharging process

Fig. 2: Cooling and condensation during the charging process and heating and evaporation during the discharging process

The heat transfer rate is calculated by the temperature difference between the solid wall and the surrounding air as in Eq. 3[25,26].

$$\dot{q} = hA\left(T - T_s\right) \tag{3}$$

The Reynolds number in a mini channel is within a laminar range under the reference condition, and the Nusselt number is known as 3.61[27, 28] in a square channel (Fig. 1) with constant heat flux. The surface heat transfer coefficient is calculated from the definition of the Nusselt number, $h = Nu \cdot k_f / w$, where w is the width of the square duct.

The mass transfer rate is calculated by the humidity ratio difference between the air stream and the saturated wall surfaces using Eq. 4[30, 31]. The mass transfer coefficient is calculated from the Lewis analogy of heat and mass transfer[29, 30].

$$\dot{m}_w = h_d A\left(W - W_{sat}\right) \tag{4}$$

The transient solid temperature is calculated by considering the sensible and latent heat transfer rates acquired from the air stream as in Eq. 5[30, 31]. The heat conduction in the axial direction is neglected.

$$M_s c_{p_s} \frac{\partial T_s}{\partial t} = \dot{q} + \dot{m}_w i_{fg} \tag{5}$$

2.3 Efficiency

The heat and moisture accumulated on the solid surface during a charging process are released into the supply air stream during a discharging process. After several cycles of calculation, it reaches a cyclic steady state.

The temperature efficiency represents the heat recovery efficiency of sensible heat. It is defined as the ratio of the indoor and outdoor temperature difference to the supply air temperature increase, as given by Eq. 6[20, 33]. As the supply air temperature varies periodically for AC-HRVs, it needs to be averaged over a discharging half-period.

$$\eta_T = \frac{\overline{T_{SA}} - T_C}{T_H - T_C} \tag{6}$$

Likely, the enthalpy efficiency can be defined as in Eq. 7[26, 31]. The enthalpy efficiency is the total efficiency of the HRV, which transfers both latent and sensible heat. The enthalpy of the supply air is averaged over a discharging half-period as shown in Eq. 8[26, 31].

$$\eta_i = \frac{\overline{i_{SA}} - i_C}{i_H - i_C} \tag{7}$$

$$\overline{i_{SA}} = \frac{1}{t_p}\int_{t_p}^{2t_p} i_{SA}(t)dt \tag{8}$$

3. Results and Discussion

The efficiencies in dry and partially wet conditions are compared for the given reference conditions by varying system parameters one by one. Fig. 3 shows the difference is appreciable, especially when the thermal storage unit is longer than 0.5 m. The longer the unit is, the greater the amount of condensation on its surfaces, which increases the enthalpy efficiency. As the length increases, the solid temperature varies over a wide range along the axial direction, and the heat transfer surface increases.

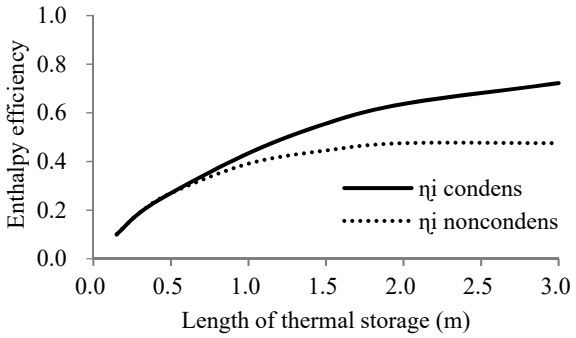

Fig. 3: Enthalpy efficiency for various lengths of thermal storage units (RH_{in}=50%, Q=200 CMH)

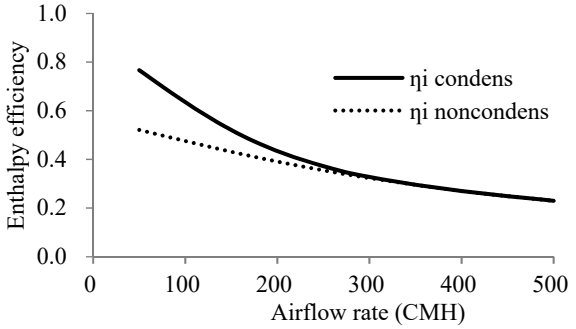

Fig. 4: Enthalpy efficiency for various airflow rates (RH_{in}=50%, L=1 m)

Figure 4 illustrates the effect of the airflow rate on enthalpy efficiency. As the airflow rate increases, the efficiency decreases. The higher the airflow, the more moisture is entrained into the channel, and more condensate should be produced[35]. However, increased airflow increases the air velocity and reduces the time duration for the air stream to interact with the channel surface. Increased airflow rate affects the discharging process similarly. The slower the airflow, the more time for moist air to condensate and evaporate, which results in higher efficiency.

The effect of indoor humidity level is shown in Fig. 5. The enthalpy efficiency decreases as the indoor relative humidity (RH) increases up to 50%, and remains nearly constant afterwards. This is because the enthalpy difference between indoor and outdoor air increases as the indoor RH increases. The amount of water content in the air also affects the amount of heat transfer[34]. However, for RH over 50%, the enthalpy efficiency slightly increases due to the contribution of the latent heat of the water vapor recovered from the condensate water accumulated on solid surfaces.

The temperature efficiency is nearly constant and decreases slowly as the condensation takes place. The latent heat contributes to increasing the enthalpy of the incoming outdoor air but reduces its temperature. The psychrometric chart in Fig. 6 explains the physical reasons regarding the effects of the parameters on efficiencies.

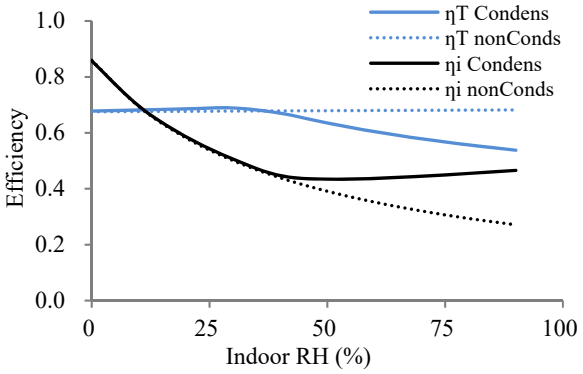

Fig. 5: Enthalpy and temperature efficiencies with respect to indoor relative humidity (L=1 m, Q=200 CMH)

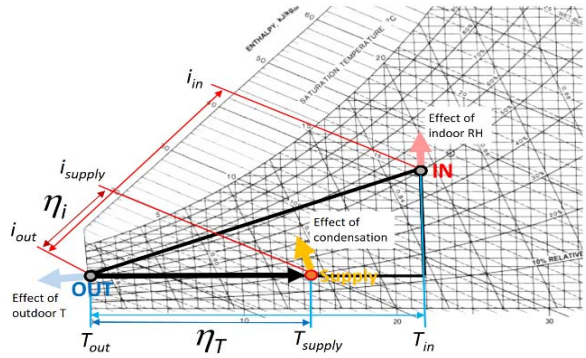

Fig.6: Psychrometric chart showing the temperature efficiency and the enthalpy efficiency.

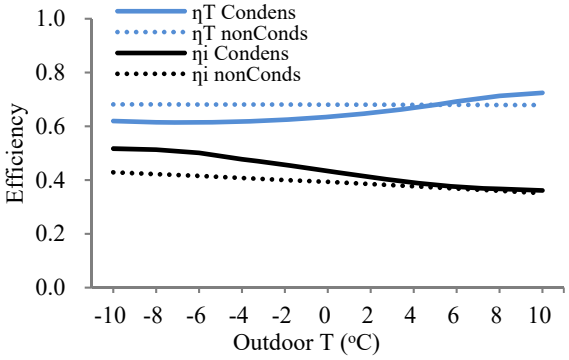

Fig. 7: Enthalpy and temperature efficiencies with respect to outdoor temperature
(RH_{in}=50%, L=1 m, Q=200 CMH)

In order to understand the physics of heat and mass transfer inside the thermal storage unit, transient temperature and moisture distributions are obtained for charging and discharging processes at cyclic steady state.

Figure 7 shows the effect of the outside air temperature. Both the temperature and the enthalpy efficiencies are nearly unaffected by the outdoor temperature for dry conditions. For wet conditions, the temperature efficiency increases slightly, but the enthalpy efficiency decreases as the outdoor temperature increases. The decreased outside air temperature increases the condensation rate, which results in greater enthalpy efficiency. This simulation is carried out with a fixed RH of both outside and inside (50%). The indoor temperature remains at 22°C.

Figure 8 shows the temperature progress that starts from a uniform initial temperature at 0ºC and then reaches cyclic steady state for the condensation case. It shows variations of inlet and outlet air temperatures and average temperature. Compared to the somewhat linear increase in temperature for the non-condensation case shown in Fig. 9, the temperature graphs show some curvatures. Even though the final temperatures are not much different, the presence of condensation affects the temperature progress due to the latent heat involved in the processes of condensation and evaporation. The efficiencies shown in the figures are obtained after initial transients fade out, usually after five cycles.

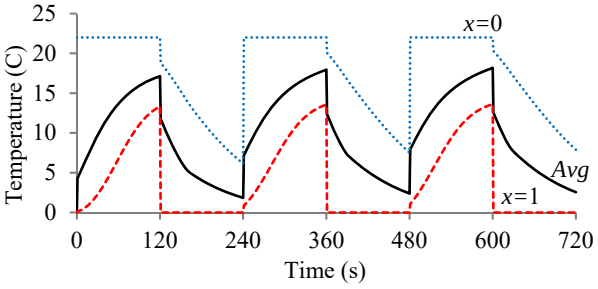

Fig. 8: Air temperature variations at inlet, outlet, and average for initial 3 cycles for the condensation case

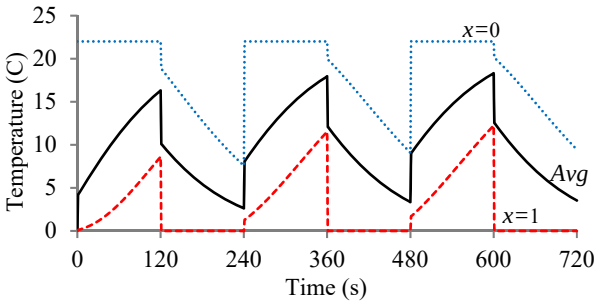

Fig. 9: Air temperature variations at inlet, outlet, and average for initial 3 cycles for the non-condensation case

Solid temperature variations are shown in Fig. 10 for the condensation case and in Fig. 11 for the non-condensation case. Initially, the solid temperatures are assumed to be 0°C at any location. With the same initial conditions, the temperature changes are smoother for the non-condensation case compared to the condensation case. However, this does not really affect the temperature changes and air enthalpy changes that pass through the thermal storage, which are the core of all the processes in this HRV.

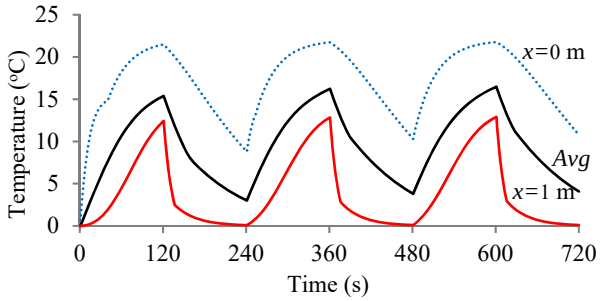

Fig. 10: Solid temperature variations of the thermal storage unit during initial 3 cycles for the condensation case

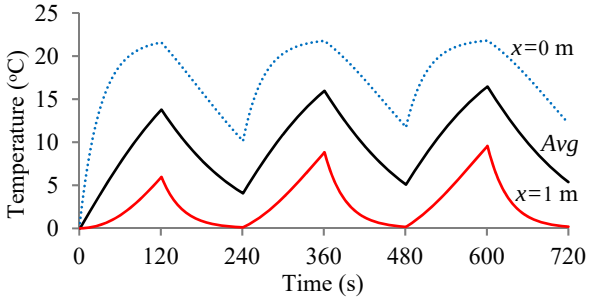

Fig. 11: Solid temperature variations of the thermal storage during initial 3 cycles for the non-condensation case

Figure 12 shows the moisture transfer rate to and from the solid surface at several locations (x = 0, 0.5, 1 m, and average) during one period after cyclic steady state is reached. Positive values mean condensation, and negative values mean evaporation. At the inlet (x = 0 m), condensation occurs at the beginning of the charging process, and then the condensate evaporates immediately afterward (t = 18 s) because the solid surface temperature becomes greater than the saturation temperature. At the outlet (x = 1 m), the rate of condensation is much greater than at the inlet starting from the beginning. It reaches the maximum at 56 s and decreases to nearly zero at the end of the charging process.

As soon as the discharging process starts, the condensate water accumulated at the end is very rapidly evaporated because of the cold dry outdoor air. It takes only 16 s to dry out completely. On average, all the condensate on the surface of the thermal storage unit is completely evaporated at 152 s. Thereafter, only the sensible heat transfers for the rest of the air supply process.

Figure 13 shows the rate of condensation or evaporation along the axial direction at several different time steps. We can see in the graph that at the initial stage (t = 1 s), condensation occurs at all the positions of the thermal storage unit until the air exits the channel. At 30 s, there is no condensation or evaporation up to x = 0.14 m. As time goes on, the dry front moves from the inlet to the right. When the flow direction is reversed at 120 s, evaporation occurs only in the range of 0.62 m < x < 0.8 m at 150 s.

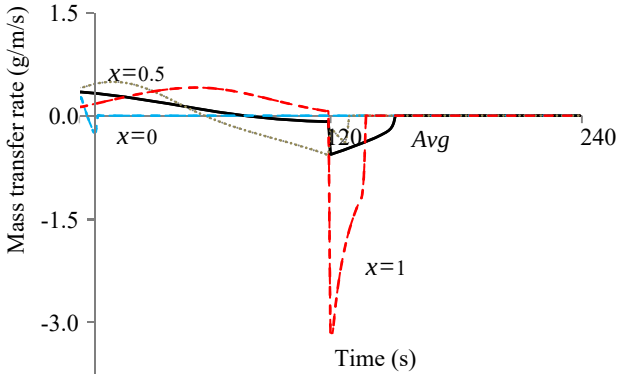

Fig. 12: The rate of condensation (or evaporation) on solid surface over one cycle.

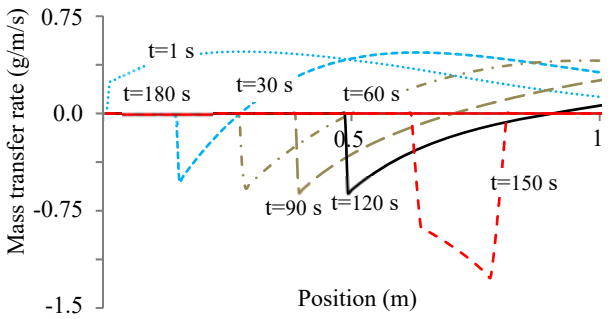

Fig. 13: The rate of condensation (or evaporation) on solid surface along the x-direction at various time steps.

Figure 14 shows the accumulated amount of condensate water remaining on the surface of the thermal storage for one cycle. At the center (x = 0.5), the accumulated mass reaches a peak at 60 s and it runs out at 128 s. At the outlet

(x = 1), it reaches a peak at the end of the charging process and decreases rapidly as soon as the discharging process starts. The maximum amount of water mass is 0.33 g/m at x = 1 m and t = 120 s, which corresponds to 2.67 μm in layer thickness. The thickness is small enough so as neither to create liquid flows in the thermal storage unit nor affects the airflow over the surface. One of the advantages of using AC-HRV is the condensed water is not steadily accumulated but dries out periodically within a cycle. A water drain is not required for most indoor and outdoor conditions.

The accumulated amount of condensate water is redrawn along the solid surface in Fig. 15. We can see from the graph that the condensate seems moving from left to right, as time goes. At the end of the charging process (t = 120 s) condensate remains only at the right half of the thermal storage. It increases to its peak at the end of the thermal storage (x = 1 m). Then all the condensate is evaporated in the exhaust process and decreases until it runs out at 152 s. This explains the previous observations in Fig. 3 where the longer the thermal storage, the greater the efficiency. Because the longer the thermal storage, the greater the condensate produced in the exhausting process which is then returned to the air that enters the room in the air supply process.

Figure 16 shows total water mass condensed in the heat exchanger element during charging and discharging processes. It shows a maximum of 14.5 g at around 80s and a sharp decrease after 120s.

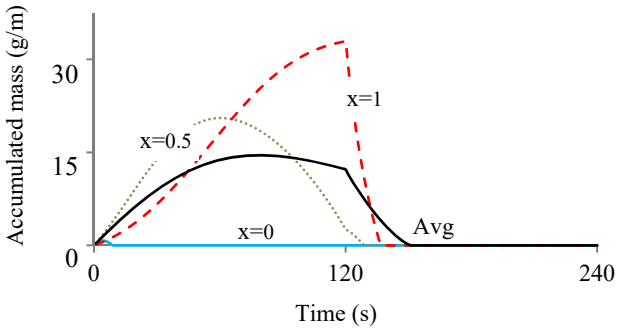

Fig. 14: Accumulated mass of water condensed on solid surface over one cycle.

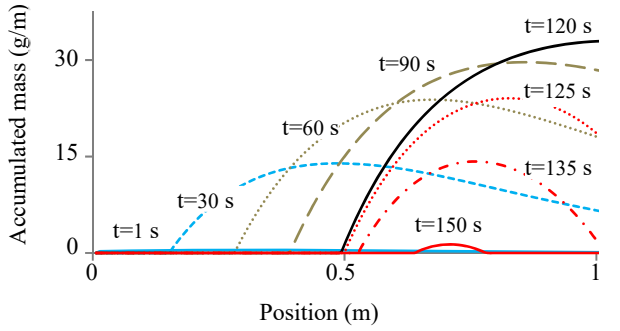

Fig. 15: Accumulated mass of water condensed on solid surface along the x-direction.

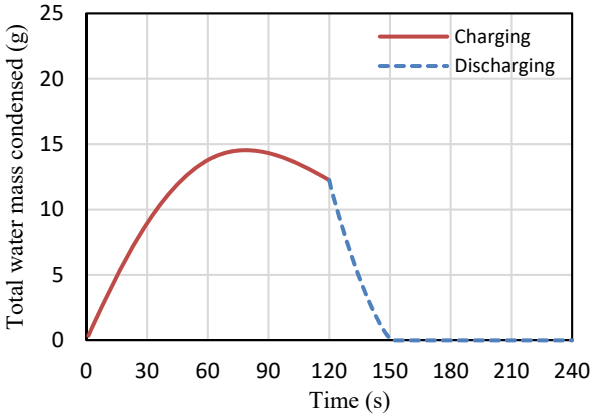

Fig. 16: Total mass present inside heat exchanger element during charging and discharging processes

4. Conclusions

A simple condensation model has been developed and successfully applied to simulate heat and moisture transfer and to calculate the enthalpy and temperature efficiencies for partially wet conditions inside the AC-HRV system. Following conclusions can be drawn from the transient heat and moisture analysis in an AC-HRV:

1. As the length of the thermal storage unit increases and the airflow rate decreases, the enthalpy efficiency increases.
2. The process of condensation and evaporation causes latent heat transfer in addition to sensible heat transfer. As the amount of condensation/evaporation increases, the enthalpy efficiency increases and the temperature efficiency decreases compared to the equivalent dry conditions.
3. As the total amount of water condensed is not significant enough during a charging process, all the condensate is dried out completely at the beginning of the discharging process for the proposed AC-HRV system.

Further research need to be conducted for various system parameters to apply to real applications.

Acknowledgements

This work was supported by the Basic Science Research Program through the NRF funded by the Ministry of Education (2016R1D1A1B01009625) and Kookmin University.

Nomenclature

A	Internal surface area per length (m^2/m)
a	Wall thickness of mini channel (m)
c_p	Specific heat capacity (J/kg/K)
D	Diameter of thermal storage unit (m)
h	Heat transfer coefficient ($W/m^2/^oC$)

h_d	Mass transfer coefficient (kg/m^2/s)
i	Enthalpy (J/kg)
L	Length of thermal storage unit (m)
M	Moisture condensed per length (kg/m)
$\dot{m}$	Mass flow rate per length (kg/s/m)
$\dot{q}$	Heat transfer rate per length (W/m)
Q	Volume airflow rate (CMH)
RH	Relative humidity (–)
T	Temperature (°C)
t	Time (s)
t_p	Half-period (s)
U	Air velocity (m/s)
x	Coordinate (m)
w	Width of mini channel (m)
W	Humidity ratio (kg_w/kg_{air})

Greek symbols

ρ	Density (kg/m^3)
η	Efficiency (–)

Subscripts

1	inlet
2	outlet
a	dry air
C	cold
fg	fluid-gas
H	hot
s	solid (thermal storage)
SA	supply air
sat	saturated
w	liquid water

References

1) N.E. Klepeis, W.C. Nelson, W.R. Ott, J.P. Robinson, A.M. Tsang, P. Switzer, J.V. Behar, S.C. Hern, and W.H. Engelmann, "The national human activity pattern survey (nhaps): a resource for assessing exposure to environmental pollutants," *J. Exp. Sci. & Env. Epidemiology*, **11** 231–252 (2001). doi: 10.1038/sj.jea.7500165.
2) D.P. Wyon, "The effects of indoor air quality on performance and productivity," *Indoor Air*, **14** (*7*) 92–101 (2004). doi: 10.1111/j.1600-0668.2004.00278.x.
3) M.H. Mahmood, M. Sultan, and T. Miyazaki, "Study on water-vapor adsorption onto polymer and carbon based adsorbents for air-conditioning applications," *Evergreen*, **6** (*3*) 215-224 (2019). doi: 10.5109/2349297.
4) ASHRAE, "Ventilation for acceptable indoor air quality," ANSI/ASHRAE Standard 62.1, 2016.
5) K. Ito, "Micro- and macro-scale measurement of fungal growth under various temperature and humidity conditions," *Evergreen*, **1** (*1*) 32-39 (2014). doi: 10.5109/1440974.
6) Y.E. Fouih, P. Stabat, P. Rivière, P. Hoang, and V. Archambault, "Adequacy of air-to-air heat recovery ventilation system applied in low energy buildings," *Energy and Buildings*, **54** 29-39 (2012). doi: 10.1016/j.enbuild.2012.08.008.
7) H. Han, M. Hatta, and H. Rahman, "Smart ventilation for energy conservation in buildings," *Evergreen*, **6** (*1*) 44-51 (2019). doi: 10.5109/2321005.
8) A. Mardiana-Idayu, and S.B. Riffat, "Review on heat recovery technologies for building applications," *Renew. and Sust. Energy Reviews*, **16** (*2*) 1241-1255 (2012). doi: 10.1016/j.rser.2011.09.026.
9) Q. Xu, S. Riffat, and S. Zhang, "Review of heat recovery technologies for building applications," *Energies*, **12** (*7*) 1285-1307 (2013). doi: 10.3390/en12071285.
10) H. Manz, and H. Huber, "Experimental and numerical study of a duct/heat exchanger unit for building ventilation," *Energy and Buildings*, **32** (*2*) 189-196 (2000). doi: 10.1016/S0378-7788(00)00043-8.
11) A. Novoselac, and J. Srebric, "A critical review on the performance and design of combined cooled ceiling and displacement ventilation systems," *Energy and Buildings*, **34** (*5*) 497-509 (2002). doi: 10.1016/S0378-7788(01)00134-7.
12) H. Han, and Y.I. Kwon, "Inhaling/exhaling heat recovery ventilator using the concept of AC ventilation," *Proc.Indoor Air*, 976-981 (2005).
13) H. Han, and Y.I. Kwon, "Inhaling/exhaling heat recovery ventilator using the concept of alternating-current ventilation," *HVAC&R Research*, **12** (*3c*) 483-459 (2006). doi: 10.1080/10789669.2006.10391212.
14) A. Mardiana, and S.B. Riffat, "Review on physical and performance parameters of heat recovery systems for building applications," *Renew. and Sust. Energy Reviews*, **28** (*2*) 174-190 (2013). doi: 10.1016/j.rser.2013.07.016.
15) O. SeppĘnen, "Ventilation strategies for good indoor air quality and energy efficiency," *Int. J. Ventilation*, **6** (*4*) 297-306 (2008). doi: 10.1080/14733315.2008.11683785.
16) J. Fernández-Seara, R. Diz, F.J. Uhía, A. Dopazo, and J.M. Ferro, "Experimental analysis of an air-to-air heat recovery unit for balanced ventilation systems in residential buildings," *Energy Conv. and Manage.*, **52** (*1*) 635-640 (2011). doi: 10.1016/j.enconman.2010.07.040.
17) C.J. Simonson, and R.W. Besant, "Energy wheel effectiveness: part I—development of dimensionless groups," *Int. J. Heat and Mass Transfer*, **42** (*12*)

2161-2170 (1999). doi: 10.1016/S0017-9310(98)00325-1.
18) T.R. Nielsen, J. Rose, and J. Kragh, "Dynamic model of counter flow air to air heat exchanger for comfort ventilation with condensation and frost formation," *App. Thermal Eng*., **29** (*2–3*) 462-468 (2009). doi: 10.1016/j.applthermaleng.2008.03.006.
19) S.H. Nam, and H. Han, "Computational modeling and experimental validation of heat recovery ventilator under partially wet conditions," *App. Thermal Eng*., **95** 229-235 (2016). doi: 10.1016/j.applthermaleng.2015.11.023.
20) H. Han, S.H. Nam, and G.S. Han, "Effect of condensation on the efficiency of heat recovery ventilators for broiler houses," *Int. J. Air-Cond. and Refrig.*, **21** (*2*) 009-019 (2013). doi: 10.1142/S2010132513500090.
21) M.I. Nizovtsev, V.Y. Borodulin, and V.N. Letushko, "Influence of condensation on the efficiency of regenerative heat exchanger for ventilation," *App. Thermal Eng*., **111** 997-1007 (2017). doi: 10.1016/j.applthermaleng.2016.10.016.
22) B.H. Jeon, J.W. Kim, S.K. Lee, Y.J. Lee, and Y.C. Ahn, "A study on the dew condensation according to the operational conditions of a heat-recovery ventilator," *Kor. J. Air-Cond. and Ref. Eng*., **25** (*10*) 529-533 (2013). doi: 10.6110/KJACR.2013.25.10.529.
23) H. Han, and M.W. Shin, "A study on heat recovery characteristics of porous media according to periodic oscillating flows," *Kor. J. Air-Cond. and Ref. Eng*., **19** (*2*) 175-182 (2007).
24) A.A. Farizi, and H. Han, "Effect of parameters of thermal storage unit for alternating current heat recovery ventilator," *Proc. Summer Conf. of Soc. of Air-Cond. and Ref. Eng. of Korea*, **6** 630-633 (2019).
25) H. Han, and M.W. Shin, "A study on heat recovery characteristics of porous media according to periodic oscillating flows," *Kor. J. Air-Cond. and Ref. Eng*., **19** (*2*) 175-182 (2007).
26) F.C. McQuiston, J.D. Parker, and D.J. Splitler, "Heating, ventilating, and air conditioning : analysis and design 6th ed.," John Wiley and Sons, 2005. https://books.google.co.kr/books?id=V_C-DwAAQBAJ&printsec=frontcover&hl=id#v=onepage&q&f=false.
27) T.L. Bergman, "Fundamentals of heat and mass transfer 8th ed.," John Wiley and Sons, 2011. https://books.google.co.kr/books?id=vvyIoXEywMoC&printsec=frontcover&hl=id#v=onepage&q&f=false.
28) Y.A. Cengel, and A.J. Ghajar, "Heat and mass transfer 5th ed.," McGraw-Hill Education, 2015. https://books.google.co.kr/books?id=B89MnwEACAAJ&dq=editions:ISBN9814595276&hl=id.
29) J.C. Kloppers, and D.G. Kröger, "The Lewis factor and its influence on the performance prediction of wet-cooling towers," *Int. J. Thermal Sciences*, **44** (*9*) 879-884 (2005). doi: 10.1016/j.ijthermalsci.2005.03.006.
30) L. Xia, M.Y. Chan, S.M. Deng, and X.G. Xu, "A modified logarithmic mean enthalpy difference (LMED) method for evaluating the total heat transfer rate of a wet cooling coil under both unit and non-unit Lewis Factors," *Int. J. Thermal Sciences*, **48** (*11*) 2159-2164 (2009). doi: 10.1016/j.ijthermalsci.2009.04.002.
31) S.K. Wang, "Handbook of air conditioning and refrigeration 2nd ed.," McGraw-Hill Education, 2001.
32) S. Sugarman, "HVAC Fundamentals," The Fairmont Press, 2005.
33) ASHRAE, "Air-to-air energy recovery," ASHRAE Handbook: HVAC Systems and Equipment Chap. 26, 2012.
34) I. Yaningsih, M.H. Mahmood, A.T. Wijayanta, T. Miyazaki, and S. Koyama, "Experimental study on dehumidification technology using honeycomb desiccant block," *Evergreen*, **5** (*2*) 11-18 (2018). doi: 10.5109/1936212.
35) B. Bakthavatchalam, K. Rajasekar, K. Habib, R. Saidur, and F. Basrawi, "Numerical Analysis of Humidification Dehumidification Desalination System," *Evergreen*, **6** (*1*) 9-17 (2019). doi: 10.5109/2320996.